PCCP

Characterization of the Simplest Hydroperoxide Ester, Hydroperoxymethyl Formate, a Precursor of Atmospheric Aerosols

Journal:	*Physical Chemistry Chemical Physics*
Manuscript ID	CP-ART-06-2019-003466.R1
Article Type:	Paper
Date Submitted by the Author:	17-Jul-2019
Complete List of Authors:	Porterfield, Jessica; Harvard Smithsonian Center for Astrophysics, Radio and Geoastronomy Lee, Kin Long ; Harvard-Smithsonian Center for Astrophysics Dell'Isola, Valentina; University of Bologna, Department of Chemistry Carroll, P.; Harvard-Smithsonian Center for Astrophysics McCarthy, Michael; Harvard-Smithsonian Center for Astrophysics,

PCCP

ARTICLE TYPE

Cite this: DOI: 00.0000/xxxxxxxxxx

Characterization of the Simplest Hydroperoxide Ester, Hydroperoxymethyl Formate, a Precursor of Atmospheric Aerosols†

Jessica P. Porterfield,*[a] Kin Long Kelvin Lee[a], Valentina Dell'Isola [b], P. Brandon Carroll[a] and Michael C. McCarthy[a]

Received Date
Accepted Date

DOI: 00.0000/xxxxxxxxxx

Atmospheric aerosols are large clusters of molecules and particulate matter that profoundly affect the Earth's radiation budget and climate. Gas-phase oxidation of volatile organic compounds is thought to play a key role in nucleation and aerosol growth, but remains poorly understood. One reaction proposed to trigger formation of condensable, low volatility organic compounds is that between Criegee intermediates and carboxylic acids to yield hydroperoxide esters. Here we isolate in high yield the simplest hydroperoxide ester, hydroperoxymethyl formate ($HOOCH_2OCHO$), as a secondary product in the ozonolysis of ethylene, and establish by rotational spectroscopy that this ester adopts a nearly-rigid cyclic structure owing to a strong hydrogen bond between the peroxy hydrogen and carbonyl oxygen. Subsequent detection of this ester in the ozonolysis of propylene and isoprene suggests that terminal alkenes readily undergo specific types of second-order oxidation reactions that have been implicated in the formation of atmospheric aerosols.

Introduction

Some of the largest uncertainty associated with modern climate models hinges on the impact of atmospheric aerosols because of their ability to scatter and absorb light and induce cloud formation[1]. Aerosols are known to be highly dynamic systems, influenced heavily by gas phase oxidation chemistry[2,3]. To fully understand the impact of atmospheric aerosols, how they initially form and chemically evolve, detailed insight into their gas and condensed phase chemistry must be achieved[4].

Heavy polar molecules, such as extra-low volatility organic compounds (ELVOCs), are believed to trigger the formation of aerosols because they are prone to facile condensation[5,6]. How relatively light volatile organics emitted from the surface of the earth in very large quantities[7] are oxidized to form such species, however, is a relatively new subject and remains largely speculative. One set of reactions that may be capable of producing molecules as heavy as ELVOCs is between Criegee intermediates[8] and carboxylic acids[6], the simplest and most fundamental of which involves carbonyl oxide (CH_2OO) and formic acid ($HCOOH$) to form hydroperoxymethyl formate ($HOOCH_2OCHO$, hereafter HPMF)[6,9,10], see Figure 1.

Experiments aimed at observation of HPMF specifically, and organic peroxides more generally, have proven challenging because peroxides are thermally labile, dissociate at relatively low temperatures, decompose catalytically in the presence of stainless steel, and easily photo-fragment. Conventional aerosol mass spectrometers, for example, operate at temperatures much too high (up to 600 °C) to characterize most peroxides[11,12]. Although there are methods for detection of peroxides by gas chromatography where long term exposure to stainless steel is necessary, secondary chemistry results in inferred rather than direct observation[13]. Furthermore it has been shown that under conditions where HPMF is believed to be present, little to no parent ion signal can be observed by photoionization mass spectrometry, and fragmentation patterns must instead be used to assign molecules based upon calculated ionization energetics[10,14–16]. Attempts to observe HPMF at infrared wavelengths have also

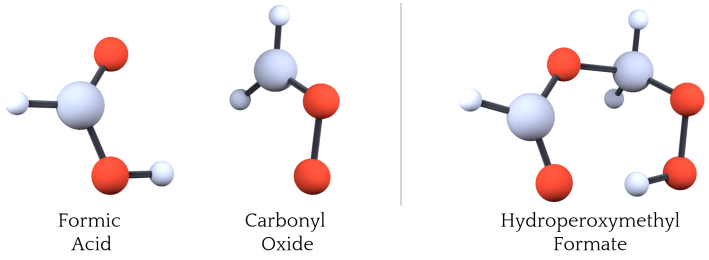

Fig. 1 The reaction between formic acid ($HCOOH$) and carbonyl oxide (CH_2OO) to form hydroperoxymethyl formate ($HOOCH_2OCHO$).

[a]*Harvard Smithsonian Center for Astrophysics, 60 Garden St, Cambridge, MA, USA; E-mail: jessica.porterfield@cfa.harvard.edu*
[b]*Dip. di Chimica "Giacomo Ciamician", Universita' di Bologna, Via F. Selmi, 2, 40126 Bologna, Italy*

been thwarted by strong overlapping vibrational bands of formic anhydride (HCO-O-HCO), a prominent dissociation product of HPMF[9,17–19].

The ozonolysis of ethylene is the simplest oxidation reaction which can generate HPMF. Because a number of products of this reaction were previously identified at high spectral resolution[20], the ozonolysis of ethylene serves as in ideal system to explore secondary chemistry more generally. Towards this end, we undertook an exhaustive spectroscopic study of this reaction using a modified pulsed reactor and chirped-pulse Fourier transform (FT) microwave spectroscopy at centimeter-wavelengths, which resulted in the detection of a number of strong unassigned rotational lines. Subsequent experiments using a cavity-enhanced spectrometer established that the majority of these lines arose from a common carrier, which we tentatively identified as HPMF on the basis of theoretical calculations of its structure. To confirm this assignment, we then extended our rotational analysis to include the two ^{13}C isotopic species, which were observed in natural abundance. To gain a deeper understanding of the role of HMPF, its production was monitored in relation to other species including formic acid, and starting with other terminal alkenes such as propylene and isoprene. Finally, we have considered the potential for OH radical chemistry from the decomposition of HPMF.

Methods and Calculations

One of the most accurate determinations of molecular structure comes from microwave spectroscopy, which is based upon the rotational pattern of a molecule. The spectrometers employed in this study have been described in considerable detail previously[21,22], so we only summarize information pertinent to the present work here. A modified pulsed valve serves as a reactor for the ozone and ethylene starting materials. It employs two capillaries which introduce the reagents at standard temperature (298 K) and pressure (1 bar) just behind the exit of the pulsed valve (see Figure 2 from Womack et al.[20]). At a flow rate of approximately 300 standard cubic centimeters per minute, ethylene (1%) and ozone (4%) (introduced via separate capillaries) are blended in the presence of argon (14%) and oxygen (81%) for of order 1 sec prior to injection into a large vacuum chamber which is maintained at low pressure ($\leq$1 x 10^{-5} Torr). Free expansion of this gas forms a supersonic jet, which rapidly cools molecules rotationally, and collisionally stabilizes highly reactive species. Roughly 3.5% of the reactive mixture is pulsed into the spectrometer[20], with the remainder exhausted into a fume hood.

As the gas mixture reaches the center of the chamber it is probed using either a cavity-enhanced Fourier-transform microwave (FTMW) spectrometer or a chirped pulse FTMW spectrometer, both of which are located in the same chamber but positioned along perpendicular axes. The chirped pulse FTMW spectrometer operates in three separate bands, 2-8, 8-18, and 18-26 GHz while the cavity-enhanced spectrometer operates continuously between 5 and 26 GHz. Using a second cavity-enhanced instrument, line measurements can be extended to 40 GHz. The most accurate line frequencies (2 kHz) are derived from cavity measurements, and these are used for least-squares fitting. Automated double resonance spectroscopy[22] is used to cross-correlate unassigned lines, and thereby determine features which arise from a common carrier.

Initial guesses for rotational constants of correlated lines are calculated using a high-speed, rigid-rotor search program based on a library of previously calculated eigenvalues. Three rotational constants are varied between 2 and 10 GHz in increments of 10 MHz, and resulting predicted transition frequencies are scored based upon proximity to the experimentally measured lines and double resonance connectivity.

Quantum chemical calculations are performed using the Gaussian '16 suite of electronic structure programs[23]. The equilibrium structures of HPMF, formic anhydride, and other stationary points are obtained using the dispersion-corrected hybrid density functional ωB97X-D[24] with a cc-pVQZ basis. Anharmonic corrections to vibrational frequencies and vibration-rotation interaction constants are calculated using second-order vibrational perturbation theory[25] (VPT2) with the same method and basis set, see Table S5. To accurately determine reaction energetics, the correlation energy is treated using the W1BD composite thermochemical scheme[26], replacing the conventional B3LYP/cc-pVTZ structure and harmonic frequencies with the ωB97X-D/cc-pVQZ structure and anharmonic zero-point energy.

Results and Discussion

A 12-16 GHz section of the chirped spectrum of the ozonolysis of ethylene under our experimental conditions is displayed in Figure 2. Only about 1/2 of the three dozen or so strong lines in the 2–26 GHz frequency range were readily assigned to products such as glycolaldehyde and formic anhydride (see Table S1). Subsequent assays established that all of the remaining unassigned lines required the presence of both ethylene and ozone, and using automated double resonance spectroscopy[22], it was soon demonstrated that a subset of these lines — eight in total — were linked together, and thus must arise from the same molecular carrier. Using the high-speed program for fitting rotational spectra[27], it was then possible to derive a set of rotational constants that reproduced these initial measurements well.

Using this initial fit, a much larger number of lines were soon found at lower and higher frequencies using a cavity-enhanced microwave spectrometer (Table S2). It is worth noting that at least one of these lines was observed previously: Womack et al.[20] (see their Figure 3) reported a strong unassigned line at 23186.69 MHz, very close in frequency to the fundamental rotational line of the Criegee intermediate (23186.49 MHz); this line is the $3_{12} \rightarrow 2_{02}$ transition of the same new molecule. By varying eight parameters in a standard asymmetric top Hamiltonian with centrifugal distortion[28], the three rotational constants and all five quartic centrifugal distortion terms, we achieved a fit rms of 6.7 kHz, roughly one-half the measurement uncertainty. Table 1 summarizes the derived rotational constants, while the complete list of spectroscopic constants is given in Table S3. The asymmetry parameter $\kappa = -0.426$, which provides an indication of the overall shape of the molecule, falls modestly close to the prolate top limit ($\kappa = -1$), while the large negative inertial defect $\Delta = -16.070$ amu Å^2, establishes the new molecule has a non-planar geometry.

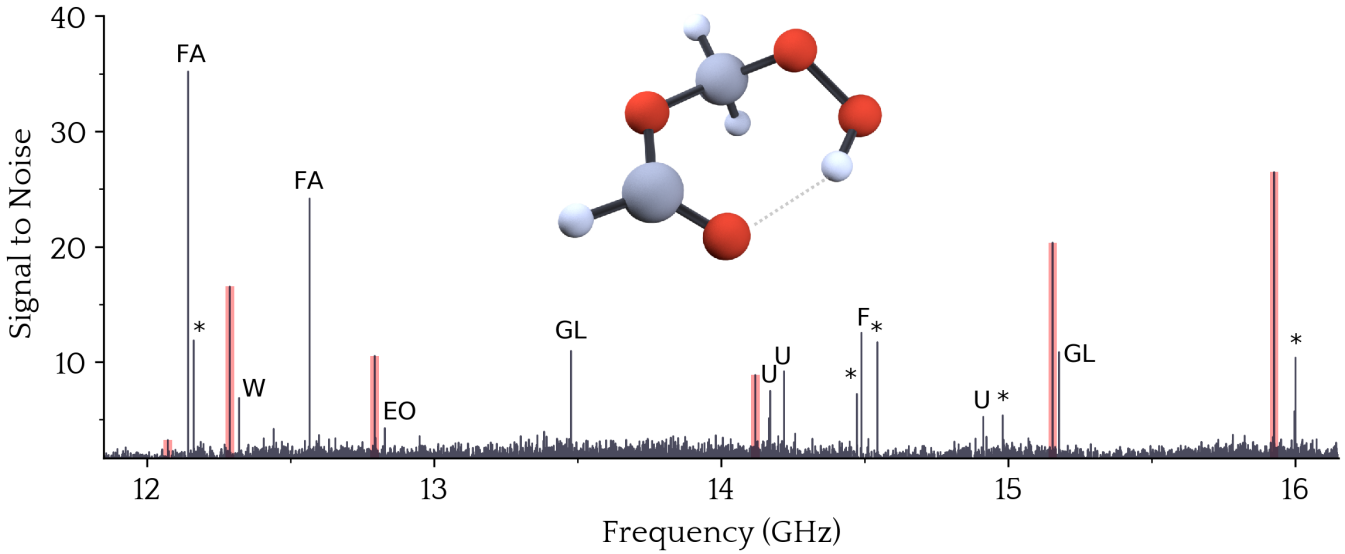

Fig. 2 A portion of the chirped microwave spectrum of the ozonolysis of ethylene between 12 and 16 GHz. Six strong transitions of hydroperoxymethyl formate, highlighted in red, were observed in this frequency range. Ultimately, a total of 65 lines were measured to 2 kHz or better between 2 and 40 GHz (Table S2) with a cavity-enhanced microwave spectrometer. The abbreviation GL refers to lines of glycolaldehyde, FA to formic anhydride, F to formaldehyde, W the water dimer, EO to ethylene oxide; U refers to unassigned features while * indicates features not observed in follow-up cavity measurements. The complete set of lines in the 2-26 GHz frequency range and their assignments is tabulated in Table S1.

The identification of the new molecule as HPMF was made using a combination of chemical intuition and inference, motivated by the knowledge of the most likely reaction products. Because its molecular structure and spectroscopic properties apparently have not been calculated prior to this work, theoretical calculations at the ωB97X-D/cc-pVQZ level of theory were performed. As indicated in Table 1, the predicted rotational constants on average agree to better than 0.1% with those derived experimentally, providing very strong evidence for the identification. The predicted and derived values of κ and Δ are also in excellent agreement, making a mis-identification highly unlikely even at this juncture. Since HPMF is chiral with sizable projections of its dipole moment along the *a*-, *b*-, and *c*-axis, all three types of transitions should be observable, which is also in agreement with our experimental findings.

Table 1 Experimental and theoretical (vibrationally averaged) rotational constants (in MHz) of hydroperoxymethyl formate, $HOOCH_2OCHO$, along with κ (unitless) and Δ (amu Å^2). Uncertainties (1σ) are in units of the last significant digit. The complete set of best-fit spectroscopic constants is provided in Table S3.

Constant	Experiment	Calculated[†]
A	5927.3044(3)	5977.1
B	3333.2483(3)	3335.5
C	2288.7557(2)	2288.1
κ	-0.426	-0.432
Δ	-16.070	-15.19

[†]At the ωB97X-D/cc-pVQZ level of theory.

Unambiguous evidence that HPMF is the molecule responsible for the lines was ultimately provided by isotopic substitution. Because lines of putative HPMF are very intense, readily detectable with a signal-to-noise ratio in excess of 200 in less than 10 sec of integration, it was possible to detect lines from the two ^{13}C isotopic species under the same experimental conditions, despite

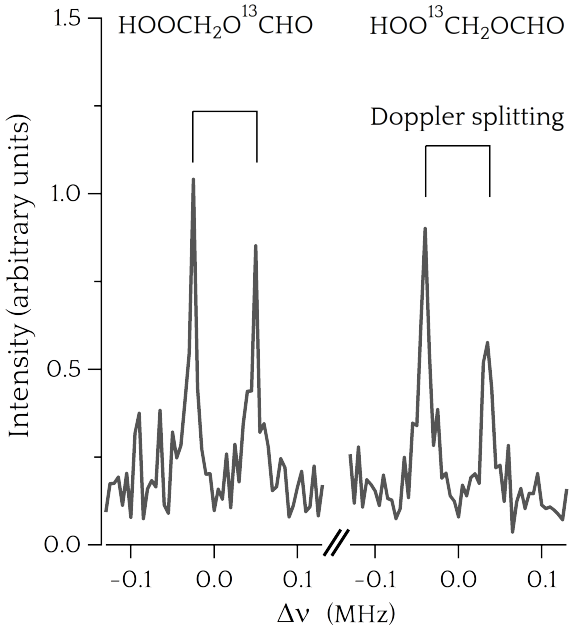

Fig. 3 The $4_{14} \rightarrow 3_{13}$ transition of $HOOCH_2O^{13}CHO$ (left) and $HOO^{13}CH_2OCHO$ (right) observed in natural abundance; the frequency axis is relative to 19749.454 MHz and 19881.197 MHz, respectively. The double-peaked line profile for each transition is instrumental in origin, arising from the Doppler effect. The integration time for each spectrum was approximately 3 min.

the low fractional abundance of this isotope (1.1%). Two sets of lines with the expected intensity (see Fig. 3) and very close in frequency to those predicted from the theoretical structure were subsequently found within 0.3% of the expected shifts, derived by scaling the theoretical rotational constants to those measured for the normal species (see Table S4). Taken in totality, there can be no doubt that the rotational spectrum of HPMF has been identified.

HPMF is a relatively large molecule, and one with a somewhat unusual geometry, however, its structural complexity was actually an aid in its characterization. For example, it has a number of allowed rotational transitions at centimeter wavelengths owing to appreciable projections of the dipole moment along each inertial axis: $\mu_a = 2.16$ D, $\mu_b = 1.90$ D, $\mu_c = 0.83$ D. Although it adopts a seven-membered ring-like structure, in which four of the six heavy atoms are oxygen, the small size of each centrifugal distortion constant indicates HPMF is very rigid, ostensibly due to a strong hydrogen bond between the peroxy hydrogen and carbonyl oxygen. A natural bond orbital analysis rationalizes the structural rigidity on the basis of large donor-acceptor interactions between the oxygen lone pair and the –OH group; the calculated interaction energy (8.9 kcal/mol) is well in excess of the low-frequency out-of-plane bending vibrational modes. As a point of comparison, this energy is almost twice that of the hydrogen bond in water dimer $(H_2O)_2$ (~5 kcal/mol)[29].

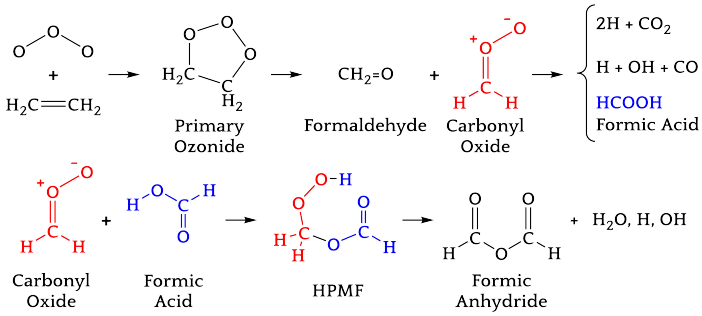

Scheme 1 The ozonolysis of ethylene, and subsequent chemistry leading to the formation of hydroperoxymethyl formate.

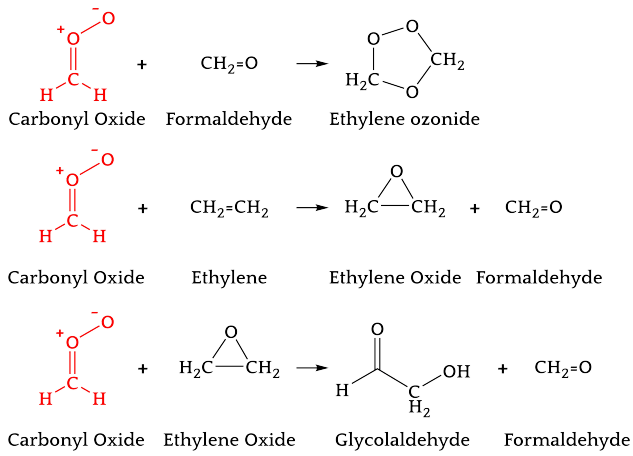

Scheme 2 Secondary chemistry observed in the ozonolysis of ethylene.

The ozonolysis of ethylene is initiated by attack of the carbon-carbon double bond by ozone to form a cyclic, five-membered ring intermediate referred to as a primary ozonide, see Scheme 1. This step is highly exothermic, resulting in rapid fragmentation of the primary ozonide to produce formaldehyde ($CH_2=O$) and carbonyl oxide (CH_2OO), the simplest Criegee intermediate. It is estimated under atmospheric conditions that roughly 40% of the Criegee intermediate is collisionally stabilized, while the remainder undergoes unimolecular arrangement or fragmentation to ultimately yield a mixture of H, CO, OH, H_2O and CO_2[30]. Rearrangement of CH_2OO can produce dioxirane or formic acid directly, however, it is likely under our experimental conditions that some formic acid is produced when the Criegee intermediate undergoes surface reactions inside the pulsed valve.

As indicated in Figure 2, several well-known ozonolysis products are observed under our experimental conditions, see Scheme 2. In the 2–26 GHz frequency range, a total of 35 lines were attributed to the products of this reaction; a complete list of line frequencies and assignments are given in Table S1. Of these, 15 are assigned: formaldehyde (2 lines), formic acid (1 line), glycolaldehyde (3 lines), formic anhydride (7 lines), water dimer (1 line), and ethylene ozonide (1 line). Secondary chemistry occurs when Criegee intermediate encounters another species, see Scheme 2.

Prior quantum chemical calculations suggest that the reaction of CH_2OO + HCOOH proceeds through barrierless association[31]. Hydrogen atom transfer from formic acid to carbonyl oxide occurs simultaneously with formation of the ester CH_2O bond, a process which we calculate to be exothermic by 171 kJ/mol. Because the formation of the primary ozonide precursor is equally or more exothermic (200 kJ/mol), and thus the Criegee intermediate is already highly energized[32], it is perhaps not surprising that formic anhydride, a primary decomposition product of HPMF[9], is easily formed, and is the second most prominent product species after HPMF in the frequency range of our broadband measurements. We calculate that the lowest energy pathway to form formic anhydride from HPMF simultaneously produces hydroxyl radical (OH). This is a barrierless elimination, requiring 111 kJ/mol input and making this process overall 60 kJ/mol exothermic relative to the starting materials. Alternatively, HPMF can eliminate water to form formic anhydride, which relative to the starting materials requires an energy input of 6 kJ/mol, and is ultimately highly exothermic (443 kJ/mol).

The general mechanism for the ozonolysis of alkenes indicates that all terminal alkenes produce carbonyl oxide, formic acid, and therefore HPMF, at some level. Isoprene [2-methyl-1,3-butadiene, $CH_2=C(CH_3)-CH=CH_2$], for example, has two C–C double bonds which will yield two distinct primary ozonides upon ozone addition, and ultimately produces three unique Criegee intermediates: methyl vinyl ketone oxide (MVK-O), methacrolein oxide (MACR-O), and carbonyl oxide. Experimental estimates of formaldehyde and either MVK-O or MACR-O production vary widely, ranging anywhere from roughly 40 to 90%[33,34]. In a mechanism mirroring carbonyl oxide to formic acid, MACR-O could rearrange to methylacrylic acid ($CH_2=C(CH_3)COOH$), for example. Ozonolysis of isoprene in the presence of carboxylic

acids has been shown to form adduct products in large yield[35], which have been classified as intermediate volatility organics[6]. Even heavier terpenes, such as α-pinene, will also likely form ELVOCs by the same mechanism at work here (see Figure 1), and these have an even higher propensity for condensation to form secondary organic aerosols[6,36].

To investigate the production of HPMF starting from other terminal alkenes, ethylene was sequentially replaced with propylene ($CH_3-CH=CH_2$) and then isoprene while the intensity of a strong line of HPMF was monitored. In both experiments, albeit not as intense, the HPMF line was easily observed with a high signal-to-noise ratio in a few seconds of integration, confirming that HPMF production in the ozonolysis of terminal alkenes is likely widespread. In addition, HPMF production relative to other products, specifically formic acid, was also monitored as a function of time. As shown in Fig. 4, a very close correlation between the two species was observed. Since HCOOH is required to form HPMF, this behavior is consistent with its formation via a simple and direct mechanism.

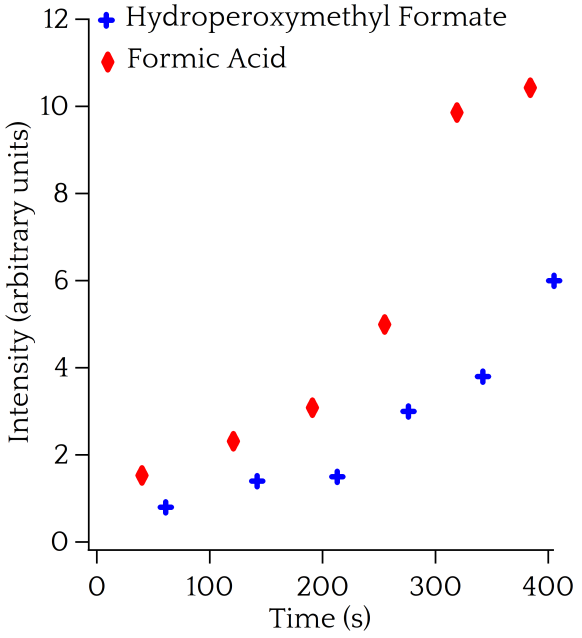

Fig. 4 Line intensities of formic acid (22471.178 MHz) and hydroperoxymethyl formate (15925.422 MHz) as a function of time in the ozonolysis of propylene, as measured by cavity-enhanced microwave spectroscopy.

The potential for OH production by decomposition of HPMF is of considerable atmospheric significance, as OH radical is a highly important catalytic oxidant. It has long been believed that ozonolysis of alkenes is an important night time source of OH radicals, due to subsequent rearrangement and decomposition of Criegee intermediates, specifically[37–39]. Other mechanisms, to our knowledge, have not yet been considered. Furthermore, organic hydroperoxides are thought to be reservoirs for atmospheric OH and HO_2 radical[40], re-emitting OH radical only in the presence of sunlight. Because the lowest energy pathway for decomposition of HPMF, a major product under our experimental conditions, produces formic anhydride and OH radical, the present work suggests another possible pathway for OH production in the ozonolysis of alkenes.

The current methodology appears well suited to produce and structurally characterize much larger esters, and other secondary products. As demonstrated here, we can produce the simplest ester in high abundance using a modified nozzle reactor, suggesting that larger secondary products can be synthesized and isolated when starting from larger terpenes. In tandem with production, we have a highly robust set of tools to identify new molecules with increasing size and structural complexity. This approach will be useful for larger esters because they have quite complicated three dimensional geometries that do not result in simple, readily identifiable rotational patterns.

Conclusion

It is remarkable that key aspects of secondary oxidation reactions as fundamental as those in the ozonolysis of ethylene, the simplest alkene, remain poorly characterized. Prior to the present work demonstrating very high yields under our experimental conditions, hydroperoxymethyl formate had eluded direct detection in a variety of ozonolysis experiments over the last fifty years. Utilizing a powerful combination of techniques, including double resonance spectroscopy, new fitting algorithms, high-level structural calculations, and isotopic substitution, the spectroscopic evidence for this ester has been established. Furthermore, we find it is present in the ozonolysis of other terminal alkenes such as propylene and isoprene, highlighting the ubiquity and the potential importance of reactions between carboxylic acids and Criegee intermediates as pathways for nucleation and growth of atmospheric aerosols. Analogous studies of larger esters and other secondary products has promise to shed light on the gap that remains between gas phase oxidation chemistry and the growth of macroscopic atmospheric particles.

Acknowledgements

The authors acknowledge NSF grant CHE-1566266 for financial support. V.D.'I. acknowledges RFO funds from the University of Bologna. P.B.C. is funded by the Simons Collaboration on the Origins of Life.

Supplementary Information Available

A complete list of experimentally observed frequencies for HPMF can be found in the Electronic Supplementary Information, along with a complete list of HPMF spectroscopic constants, ^{13}C isotopologue observed frequencies and assignments, and harmonic and anharmonic analysis of HPMF.

Notes and references

1 I. Riipinen, J. Pierce, T. Yli-Juuti, T. Nieminen, S. Häkkinen, M. Ehn, H. Junninen, K. Lehtipalo, T. Petäjä, J. Slowik *et al.*, *Atmospheric Chemistry and Physics*, 2011, **11**, 3865.

2 M. Ehn, J. A. Thornton, E. Kleist, M. Sipilä, H. Junninen, I. Pullinen, M. Springer, F. Rubach, R. Tillmann and B. e. a. Lee, *Nature*, 2014, **506**, 476–479.

3 J. L. Jimenez, M. Canagaratna, N. Donahue, A. Prevot,

Q. Zhang, J. H. Kroll, P. F. DeCarlo, J. D. Allan, H. Coe, N. Ng *et al.*, *Science*, 2009, **326**, 1525–1529.

4 B. R. Bzdek and J. P. Reid, *The Journal of Chemical Physics*, 2017, **147**, 220901.

5 J. H. Kroll and J. H. Seinfeld, *Atmospheric Environment*, 2008, **42**, 3593–3624.

6 R. Chhantyal-Pun, B. Rotavera, M. R. McGillen, M. A. H. Khan, A. J. Eskola, R. L. Caravan, L. Blacker, D. P. Tew, D. L. Osborn, C. J. Percival *et al.*, *ACS Earth and Space Chemistry*, 2018, **2**, 833–842.

7 A. Guenther, C. N. Hewitt, D. Erickson, R. Fall, C. Geron, T. Graedel, P. Harley, L. Klinger, M. Lerdau, W. McKay *et al.*, *Journal of Geophysical Research: Atmospheres*, 1995, **100**, 8873–8892.

8 R. Criegee, *Angewandte Chemie International Edition in English*, 1975, **14**, 745–752.

9 P. Neeb, O. Horie and G. K. Moortgat, *Chemical Physics Letters*, 1995, **246**, 150–156.

10 O. Welz, A. J. Eskola, L. Sheps, B. Rotavera, J. D. Savee, A. M. Scheer, D. L. Osborn, D. Lowe, A. Murray Booth and P. e. a. Xiao, *Angewandte Chemie International Edition*, 2014, **53**, 4547–4550.

11 G. I. Gkatzelis, T. Hohaus, R. Tillmann, I. Gensch, M. Müller, P. Eichler, K.-M. Xu, P. Schlag, S. H. Schmitt, Z. Yu *et al.*, *Atmospheric Chemistry and Physics*, 2018, **18**, 12969–12989.

12 M. Canagaratna, J. Jayne, J. Jimenez, J. Allan, M. Alfarra, Q. Zhang, T. Onasch, F. Drewnick, H. Coe, A. Middlebrook *et al.*, *Mass Spectrometry Reviews*, 2007, **26**, 185–222.

13 A. S. Hasson, G. Orzechowska and S. E. Paulson, *Journal of Geophysical Research: Atmospheres*, 2001, **106**, 34131–34142.

14 K. Moshammer, A. W. Jasper, D. M. Popolan-Vaida, A. Lucassen, P. Diévart, H. Selim, A. J. Eskola, C. A. Taatjes, S. R. Leone, S. M. Sarathy *et al.*, *The Journal of Physical Chemistry A*, 2015, **119**, 7361–7374.

15 A. Rousso, N. Hansen, A. Jasper and Y. Ju, *Physical Chemistry Chemical Physics*, 2019.

16 Z. Wang, O. Herbinet, N. Hansen and F. Battin-Leclerc, *Progress in Energy and Combustion Science*, 2019, **73**, 132–181.

17 F. Su, J. G. Calvert and J. H. Shaw, *The Journal of Physical Chemistry*, 1980, **84**, 239–246.

18 J. Thamm, S. Wolff, W. Turner, S. Gäb, W. Thomas, F. Zabel, E. Fink and K. Becker, *Chemical Physics Letters*, 1996, **258**, 155–158.

19 P. Neeb, O. Horie and G. K. Moortgat, *The Journal of Physical Chemistry A*, 1998, **102**, 6778–6785.

20 M. C. McCarthy, L. Cheng, K. N. Crabtree, O. Martinez Jr, T. L. Nguyen, C. C. Womack and J. F. Stanton, *The Journal of Physical Chemistry Letters*, 2013, **4**, 4133–4139.

21 M. C. McCarthy, W. Chen, M. J. Travers and P. Thaddeus, *The Astrophysical Journal Supplement Series*, 2000, **129**, 611.

22 M.-A. Martin-Drumel, M. C. McCarthy, D. Patterson, B. A. McGuire and K. N. Crabtree, *The Journal of Chemical Physics*, 2016, **144**, 124202.

23 M. J. Frisch, G. W. Trucks, H. B. Schlegel, G. E. Scuseria, M. A. Robb, J. R. Cheeseman, G. Scalmani, V. Barone, G. A. Petersson, H. Nakatsuji, X. Li, M. Caricato, A. V. Marenich, J. Bloino, B. G. Janesko, R. Gomperts, B. Mennucci, H. P. Hratchian, J. V. Ortiz, A. F. Izmaylov, J. L. Sonnenberg, D. Williams-Young, F. Ding, F. Lipparini, F. Egidi, J. Goings, B. Peng, A. Petrone, T. Henderson, D. Ranasinghe, V. G. Zakrzewski, J. Gao, N. Rega, G. Zheng, W. Liang, M. Hada, M. Ehara, K. Toyota, R. Fukuda, J. Hasegawa, M. Ishida, T. Nakajima, Y. Honda, O. Kitao, H. Nakai, T. Vreven, K. Throssell, J. A. Montgomery, Jr., J. E. Peralta, F. Ogliaro, M. J. Bearpark, J. J. Heyd, E. N. Brothers, K. N. Kudin, V. N. Staroverov, T. A. Keith, R. Kobayashi, J. Normand, K. Raghavachari, A. P. Rendell, J. C. Burant, S. S. Iyengar, J. Tomasi, M. Cossi, J. M. Millam, M. Klene, C. Adamo, R. Cammi, J. W. Ochterski, R. L. Martin, K. Morokuma, O. Farkas, J. B. Foresman and D. J. Fox, *Gaussian 16 Revision A.01*, 2016.

24 J.-D. Chai and M. Head-Gordon, *Physical Chemistry Chemical Physics*, 2008, **10**, 6615–6620.

25 V. Barone, *The Journal of Chemical Physics*, 2004, **122**, 014108.

26 E. C. Barnes, G. A. Petersson, J. A. Montgomery, M. J. Frisch and J. M. L. Martin, *Journal of Chemical Theory and Computation*, 2009, **5**, 2687–2693.

27 B. Carroll, 74th International Symposium on Molecular Spectroscopy, 2019.

28 H. M. Pickett, *Journal of Molecular Spectroscopy*, 1991, **148**, 371–377.

29 M. W. Feyereisen, D. Feller and D. A. Dixon, *The Journal of Physical Chemistry*, 1996, **100**, 2993–2997.

30 T. L. Nguyen, H. Lee, D. A. Matthews, M. C. McCarthy and J. F. Stanton, *The Journal of Physical Chemistry A*, 2015, **119**, 5524–5533.

31 B. Long, J.-R. Cheng, X.-f. Tan and W.-j. Zhang, *Journal of Molecular Structure: THEOCHEM*, 2009, **916**, 159–167.

32 L. B. Harding and W. A. Goddard III, *Journal of the American Chemical Society*, 1978, **100**, 7180–7188.

33 T. B. Nguyen, G. S. Tyndall, J. D. Crounse, A. P. Teng, K. H. Bates, R. H. Schwantes, M. M. Coggon, L. Zhang, P. Feiner, D. O. Milller *et al.*, *Physical Chemistry Chemical Physics*, 2016, **18**, 10241–10254.

34 J. P. Porterfield, S. Eibenberger, D. Patterson and M. C. McCarthy, *Physical Chemistry Chemical Physics*, 2018, **20**, 16828–16834.

35 Y. Sakamoto, R. Yajima, S. Inomata and J. Hirokawa, *Physical Chemistry Chemical Physics*, 2017, **19**, 3165–3175.

36 K. Sato, Y. Fujitani, S. Inomata, Y. Morino, K. Tanabe, S. Ramasamy, T. Hikida, A. Shimono, A. Takami, A. Fushimi *et al.*, *Atmospheric Chemistry and Physics*, 2018, **18**, 5455–5466.

37 R. Gutbrod, E. Kraka, R. N. Schindler and D. Cremer, *Journal of the American Chemical Society*, 1997, **119**, 7330–7342.

38 N. M. Donahue, J. H. Kroll, J. G. Anderson and K. L. Demerjian, *Geophysical Research Letters*, 1998, **25**, 59–62.

39 T. Malkin, A. Goddard, D. Heard and P. Seakins, *Atmospheric*

Chemistry and Physics, 2010, **10**, 1441–1459.

40 P. D. Lightfoot, R. Cox, J. Crowley, M. Destriau, G. Hayman, M. Jenkin, G. Moortgat and F. Zabel, *Atmospheric Environment. Part A. General Topics*, 1992, **26**, 1805–1961.